Electrochimica Acta 421 (2022) 140427

Contents lists available at ScienceDirect

Electrochimica Acta

journal homepage: www.journals.elsevier.com/electrochimica-acta

Ionomer immobilized onto nitrogen-doped carbon black as efficient and durable electrode binder and electrolyte for polymer electrolyte fuel cells

Won Young Choi [a,b,1], Dong Jun Seo [a,c,1], Hyunguk Choi [a,b], Myeong Hwa Lee [a,d], Seo Won Choi [a,e], Young Gi Yoon [a], Tae Young Kim [f,*], Hansung Kim [c,*], Chi-Young Jung [a,*]

[a] Fuel Cell Research and Demonstration Center, Hydrogen Energy Research Division, Korea Institute of Energy Research (KIER), Jeollabuk-do 56332, South Korea
[b] Department of Chemical Engineering, Hanyang University, Seoul 04763, South Korea
[c] Department of Chemical and Biomolecular Engineering, Yonsei University, Seoul 03722, South Korea
[d] Department of Energy Storage and Conversion Engineering, Chonbuk National University, Jeollabuk-do 54596, South Korea
[e] Graduate School of Energy Convergence, Institute of Integrated Technology, Gwangju Institute of Science and Technology, Gwangju 61005, South Korea
[f] Fuel Cell Research and Development Division, TerraLIX Company, Jeollabuk-do 54596, South Korea

ARTICLE INFO

Keywords:
Polymer electrolyte fuel cell electrode
Ionomer immobilized onto nitrogen-doped carbon black
ORR activity
Mass transport resistance
Carbon support degradation

ABSTRACT

An implementation of the polymer electrolyte fuel cell (PEFC) electrode, composed of the perfluorinated sulfonic acid (PFSA) ionomer with unprecedented uniform distribution, has recently gained a great attention due to its positive impact on the cell performance as well as durability. However, an issue with the conventional electrodes is a stronger adsorption of sulfonate terminal groups specifically onto Pt catalyst than carbon black (CB) support, that accelerates an inhomogeneous distribution of the PFSA ionomer. In this work, we report a novel PEFC electrode by introducing the ionomer immobilized onto nitrogen-doped carbon black (I/NCB) as electrode binder as well as electrolyte. The carbon atoms adjacent to nitrogen allow a considerable attraction with sulfonated groups over the NCB surfaces, which creates more homogeneous distribution of ionomer when compared with Pt/CB in the conventional electrode. As compared with the conventional electrode, the electrode employing I/NCB presents a superior activity towards oxygen reduction reaction (Pt mass activity increased from 91.3 to 139.6 A g^{-1}) and mass-transport characteristics (mass-transport resistance decreased from 65.9 to 45.5 mΩ cm^2), with the cell current density enhanced by 23% at 0.6 V. The enhanced cell durability is confirmed by less degradation in the electrochemically available surface area after the accelerated stress test of carbon support, mainly attributed to the promoted stability of NCB over CB. Given the advances in both performance and durability, the proposed electrode architecture based on I/NCB may provide an alternative pathway in obtaining better electrode kinetics and O_2 transport, along with an exceptional resistivity towards the carbon support degradation.

1. Introduction

Thanks to the green hydrogen opportunities, the polymer electrolyte fuel cells (PEFCs) have emerged as one of the most promising alternatives to the conventional power generators for both stationary and transportation applications [1–3]. For widespread use of this technology, however, there still exist critical issues including sluggish kinetics of oxygen reduction reaction (ORR) and enlarged resistance of oxygen molecular transport [4]. It is widely accepted that these drawbacks are primarily driven by strong adsorption of perfluorinated sulfonic acid (PFSA) ionomers, that acts as not only an electrode binder but also an electrolyte, onto the platinum (Pt) catalysts [5,6]. Firstly, the sulfonate anion groups ($-SO_3^-$) in the side chain of ionomer adsorb specifically onto the Pt surface while expelling water molecules pre-adsorbed at lower potentials, which lead to a significant reduction in the surface utilization of Pt [7]. Secondly, the confinement effect with an assistance of strong adsorption of ionomer onto Pt increases stiffness of the backbone and thus aggravate the transportation of O_2 [8,9]. Moreover, the enhanced ORR activity obtained from the state-of-the-art catalyst materials, with alloy, core-shell and nano-frame structures, lead to a severe catalyst poisoning by even stronger adsorption of ionomer [10]. Thus, in the last decade, one reliable strategy to address this issue has been exploring the

* Corresponding authors.
E-mail addresses: kty@terralix.com (T.Y. Kim), elchem@yonsei.ac.kr (H. Kim), cyjung@kier.re.kr (C.-Y. Jung).
[1] These authors contributed equally to this work.

https://doi.org/10.1016/j.electacta.2022.140427
Received 3 January 2022; Received in revised form 21 March 2022; Accepted 22 April 2022
Available online 25 April 2022

impacts of morphology, distribution and mass loadings of ionomer on the performance of ORR electrode, besides the enhancement of catalyst materials.

In the conventional ORR electrode, the PFSA ionomer is unevenly distributed onto the Pt/CB catalysts, due to the severe agglomeration of ionomer in the dispersion [11,12]. This leads to a drastic reduction in Pt utilization at lower ionomer contents and a notable increase in O_2 transport resistance at higher ionomer contents. To this end, various approaches have been made to give the PEFC electrode tailored with ionomer homogeneously distributed onto the Pt/CB catalyst. Significant efforts have been made to improve the ionomer distribution via design of dispersing solvents, as the structure of the ionomer agglomerates in the dispersion is resulted by the interaction between the ionomer and solvent molecules [13–20]. Welch et al. firstly showed the morphology of PFSA ionomer has significantly varied after dispersed in different types of solvents [13]. Specifically, the Nafion ionomers have structured cylindrical particles in 1,2,3-propanetriol and random coil-shaped particles in 1-methyle-2-pyrrolidinone, while highly-solvated ionomer particles are formed in water-isopropyl alcohol (IPA) mixture. Subsequently, Ngo et al. have demonstrated that the reduction of IPA concentration is clearly helpful in homogenizing the ionomer distribution in the electrode, and thus improves the fuel cell performance [14,15]. In this regards, various organic solvents, such as alcohols, acetates and glycols, have been employed in the electrode slurry, in order to obtain better dispersion [16–19]. Inspired from the above works, Orfanidi et al. and Shahgaldi et al. investigated the effect of dispersing solvent compositions and ionomer loadings on homogeneity of both low and high equivalent weight (EW) ionomers, in a hope for low Pt-loaded electrode operating at higher temperature and lower humidity environments [20,21]. The resultant electrode has succeeded in achieving better fuel cell performance reaching as high as 1.75 A cm^{-2} at a cell potential of 0.6 V, with the optimized amount of water contents (16 wt.%) in the electrode slurry.

Substantial attempts have been made with exploitation of the microstructures and surface properties of carbon supports, in order to obtain more homogeneous distribution of ionomer onto the ORR electrode [22–28]. At an early stage, the Pt catalysts deposited onto the interior surfaces of carbon supports have aggravated the catalyst utilization efficiency due to a drastic reduction in the effective surface area [22,23]. The effect of carbon support microstructures, with less amount of interior surfaces, on the PFSA ionomer distribution and the resultant cell performance was investigated thoroughly. However, Yarlagadda et al. have recently demonstrated that Pt catalysts deposited onto the exterior surfaces of carbon supports are prone to the catalyst poisoning by sulfonate moieties in the PFSA ionomer; hence, the carbon supports with internal porosity nearby exterior surfaces that may protect Pt particles and at the same time give accessibility to O_2 is more favorable [24]. To this end, the carbon support was functionalized by elements with higher electronegativity, such as amine groups (-NH_x) and nitrogen dopants (-N-), in order to obtain more homogeneous distribution of PFSA ionomer via Coulombic interaction with sulfonate groups in the sidechain [25–27]. To further improve the dispersibility of ionomer, the supercritical fluid conditions were applied to the electrode slurry for higher solvation and mass-transport characteristics [28]. Several important parameters in the electrode manufacture process, such as hot-pressing temperatures and duration, are also explored to unravel the impact of ionomer layer on the fuel cell performance [29,30]. However, despite these efforts, no direct evidence has been found for more uniform distribution of ionomer in the resultant electrodes, except considerable enhancements in the fuel cell performance. Moreover, a severe agglomeration of ionomer was inevitable during the deposition and post-deposition annealing processes, where the electrode slurry became more concentrated with lesser degree of freedom [31].

To properly address the above issue, anchoring ionomer onto an additional carbonaceous material, other than that supporting Pt catalysts, can be an effective route in obtaining the enhanced ORR electrode kinetics with higher stability [32]. Herein, we, for the first time, report the ionomer immobilized onto nitrogen-doped carbon black (I/NCB) and employment of this material as an electrolyte for the PEFC electrode. The proposed material can be simply mass-produced by deposition of PFSA ionomer onto the nitrogen-doped carbon black (NCB), that is prepared via the soft nitriding process [33]. Unlike the previous literatures regarding the microstructural configuration of conventional electrode [24,34], the resultant electrode may lead to the dramatic improvements in both ORR activity and O_2 transport by mitigating the specific adsorption and severe agglomeration of ionomer onto the Pt surfaces, mainly attributed by the immobilization of ionomer onto CB or NCB. After the use of I/NCB in the electrode, a superior cell durability is also expected towards the carbon support degradation, due to high graphitization of NCB that supports ionomer. The physicochemical property and nanoscale morphology of I/NCBs have been firstly characterized, then followed by microstructural exploration of the resultant electrode. Finally, the electrochemical properties of PEFC electrodes employing I/CB and I/NCB when compared with the conventional one, to highlight the role of I/NCB on the fuel cell performance as well as durability.

2. Experimental

2.1. Synthesis of ionomer immobilized onto N-doped carbon black (I/NCB)

The NCB was synthesized via soft nitriding method originally reported by Liu et al., owing to its scalability and eco-friendliness [33]. 1 g of the as-received carbon black (Vulcan XC-72R, Cabot Corp., 237 m^2 g^{-1}) was first acid-treated with a mixture of H_2SO_4 and HNO_3 at molar ratio of 1 to 2 at 120 °C for 6 h. Subsequently, the acid-treated carbon black was dispersed into 5 g of 30 wt.% aqueous solution of Urea, followed by magnetic stirring over 12 h to ensure a complete wetting. The dispersion was coated onto an alumina boat drop by drop. After a mild drying in the convection oven, the boat was placed in the center position of tube furnace and heat-treated at 400 °C with an elevation rate of 5 °C min^{-1} under N_2 atmosphere. The reaction time was fixed to 1 h. After cool down, the NCB powder was rinsed with deionized water and ethanol more than 5 times for a complete removal of residual urea. Finally, the PFSA ionomer was immobilized onto the NCB by physical entanglement. 1 g of the as-prepared NCB was added into 2.2 g of 25 wt.% PFSA ionomer dispersion (D2020, Ion Power, EW=1000 g mol^{-1}) and 69.6 g of the mixture solvent consisting of deionized water and 2-propanol. The dispersion was ultra-sonicated and magnetically stirred over 24 h. The slurry was 2x concentrated by thermal heating during a vigorous ultra-sonication, then followed by freeze-drying at −60 °C until gray colored carbon powder is achieved. The resultant powder was rinsed with deionized water and ethanol more than 3 times for a complete removal of unattached ionomer. The as-prepared I/NCB was dried in a convection oven at 60 °C for 24 h prior to further characterization.

2.2. Fabrication of membrane electrode assembly

All the membrane electrode assembly (MEA) samples were fabricated by modified decal-transfer method [35]. The cathode electrode slurry was prepared by dispersing 0.62 g of Pt/CB catalyst (TEC10V40E, TKK, 37.4 wt.%) into 3.27 g of mixture solvent composed of deionized water and 2-propanol with 1:2 vol ratio, then finally adding 0.57 g of I/CB or I/NCB as electrode binder and electrolyte. No additional amount of PFSA ionomer was added into the mixture. The dispersion was vigorously sonicated for 1 h before the electrode deposition. Then, the resultant slurry was deposited onto the substrate film by the blade-coating method, with the substrate gap of 60 μm and blade speed of 5 mm s^{-1} using an automatic coater (ZAA 2300, Zehntner, Double Sided Glass Plate) with the mounted infrared radiant heater (IRE135-M, Iwasaki Electric, 220 × 10.5 mm^2) until the Pt mass loading of 0.2 mg

cm^{-2} is reached, followed by a complete drying in the convection oven at 70 °C for 12 h. For the reference, the anode electrode slurry was fabricated by mixing 0.62 g of Pt/CB catalyst with 5 wt.% PFSA ionomer dispersion (D520, Ion Power, EW=1000 g mol^{-1}) to have ionomer-to-carbon ratio of 0.6, followed by identical coating procedure given above. The electrode coated on the decal substrate was successfully transferred onto Nafion membrane (NRE211, Ion Power, EW=1100 g mol^{-1}) by hot-pressing the membrane-electrode assembly at 110 °C and 100 bar for 10 min. For the benchmark, the conventional electrode composed of Pt/CB catalyst and PFSA ionomer, with identical Pt and ionomer mass loadings, was fabricated by the above procedure. Finally, the decal substrate film was peeled off from the MEA after cool down. The resultant MEAs were then kept in the desiccator filled with pure N_2 below 20% RH before further characterization.

2.3. Physicochemical characterization

High resolution transmission electron microscopy (HR-TEM, Thermo Fisher Scientific, Titan Krios G3) was conducted to investigate the morphology of NCB and I/NCB. Field emission scanning electron microscopy (FE-SEM, JSM-7900F, JEOL) was also performed to investigate the microstructures on top and cross-section surfaces of the electrodes. Energy dispersive X-ray spectrometry (EDX) analyses were combined with both TEM and SEM to capture the distribution of PFSA ionomer. In addition, the surface composition was analyzed by X-ray photoelectron spectroscopy (XPS, Kratos, Axis Ultra DLD) with Mg Ka radiation (1253.6 eV), where the spectrum was calibrated to give the C1s signal at 284.5 eV. Thermogravimetric analysis (TGA) was also conducted by heating the samples in N_2 gas at a constant rate of 10 °C min^{-1} up to 800 °C.

The electrode porosity with pore size distribution was analyzed by mercury intrusion porosimetry (MIP, Micrometrics, ASAP 2020) at pressures ranging from 0.1 to 60,000 psi. All the MEA samples were cut into more than 50 slices with an electrode area of 1 cm^2 and weighed before characterization. The electrode porosity is calculated based on the volume of solely electrode that is obtained by substracting thickness of the Nafion membrane from thickness of the overall MEA [36].

2.4. Electrochemical characterization

A PEFC unit cell was assembled by placing the MEA sample between two gas diffusion layers (GDL), which was then sandwiched by two unipolar plates with triple-serpentine gas flow channels. Commercial carbon papers coated with the microporous layer on one side (34BC, SGL Corp., 315 μm thick) were applied as GDL. The electrode area was ca. 25 cm^2. The i-V performance was recorded under the cell temperature of 80 °C and humidity of 100% RH, using a fuel cell test station (G-20, Greenlight Innovation, $P = 100$ W) [37]. Stoichiometric ratios of H_2 and air were set to 1.5 and 2.0, respectively. Before characterization, the cell was conditioned with a step-wise cycling of cell voltages from 0.3 to 0.8 V by 0.1 V at every 5 min until the i-V performance is stabilized [38]. After the cell performance measurement, EIS analysis were carried out at 1.0 A cm^{-2} using an impedance analyzer (Reference 3000, Gamry, 30 K Booster). The alternating current of disturbance amplitude was fixed at 10% of the direct current applied to the cell at the frequencies ranging from 100 kHz to 0.1 Hz [39]. The ORR activity on MEA level was obtained at a cell voltage of 0.9 V from the iR-corrected cell performance with H_2 and O_2 at 80 °C. For the CV analysis, the 99.999% H_2 and N_2 gas were added to the cell at 100% RH. The charge involved in H adsorption was used to calculate the ECSA after correcting for the influence of double-layer charging and discharging, and H_2 evolution peaks below 0.08 V (vs RHE). The potential was cycled from 0.05 to 1.20 V at a scan rate of 50 mV s^{-1}.

The carbon-support corrosion durability is remarkably challenging in the PEFC electrode for light-duty vehicle because the cathode electrode is exposed to highly oxidizing condition during operation.

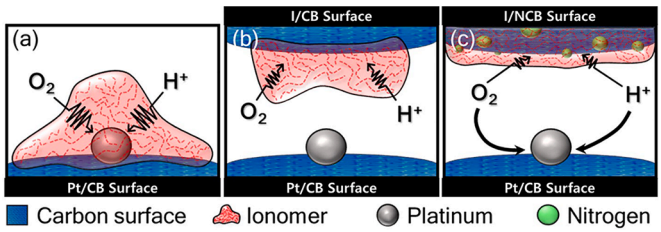

Fig. 1. Conceptual illustration of the PFSA ionomer distribution in the PEFC electrode – Pt/CB catalysts are hybridized with (a) PFSA ionomer (Bottom: Pt/CB), (b) I/CB (Top: I/CB, Bottom: Pt/CB) and (c) I/NCB (Top: I/NCB, Bottom: Pt/NCB). As shown in Fig. 1(c), more homogeneous distribution of ionomer is projected after the use of I/NCB in the electrode.

Adsorbed H_2O is the oxidant species in the carbon support corrosion reaction as expressed in Eqs. (1)–(3).

$$C + 2H_2O \rightarrow CO_2\uparrow + 4H^+ + 4e^- \quad (0.207\ V\ vs.\ RHE) \tag{1}$$

$$C + H_2O \rightarrow CO + 2H^+ + 2e^- \quad (0.518\ V\ vs.\ RHE) \tag{2}$$

$$CO + H_2O \rightarrow CO_2\uparrow + 2H^+ + 2e^- \quad (-0.103\ V\ vs.\ RHE) \tag{3}$$

To accelerate the carbon corrosion rate while maintaining the Pt dissolution rate, the AST was carried out at the cathode potentials ranging from 1.0 to 1.5 V with scan rate of 500 mV s^{-1}, at a cell temperature of 80 °C for 4000 cycles with H_2 and N_2 gas supply for the anode and cathode, respectively (US DOE Protocol) [40]. The humidity of both H_2 and N_2 gasses maintained at 100% RH as H2O is reactant in the carbon corrosion reactions. Finally, the cell was re-activated by the identical conditioning procedure with fully humidified H_2 and air gasses for 24 h before further electrochemical characterizations.

3. Results and discussion

3.1. Physical concept of the PEFC electrode with I/NCB as electrolyte

In the typical PEFC electrode, it is now widely accepted that the PFSA ionomer is unevenly distributed onto the Pt/CB catalyst, mainly due to the strong attractive interaction between Pt and sulfonate groups in the ionomer [41]. Hence, a simple approach is required to obtain more homogeneous distribution of ionomer. Fig. 1 shows the schematic illustration of variations in ionomer distribution after the employment of I/NCB in the electrode. In case without I/NCB, the ionomer layer deposited onto Pt catalyst is more likely to be thicker than that deposited onto CB support, as shown in Fig. 1(a). This will lead to the severe aggravations in the ORR activity and O_2 mass-transport characteristics. In contrast, the segregation of ionomer from Pt catalytic surfaces may provide a simple but effective approach for an improved PEFC performance when the I/NCB is applied as binder and electrolyte into the electrode (Fig. 1(b) and (c)). Particularly, when the ionomer is supported onto NCB, the sufficient numbers of carbon atoms adjacent to nitrogen dopant may attract the sulfonate groups in the sidechain of ionomer, due to the Coulombic interaction between them [27]. Hence, this results in more homogeneous distribution of ionomer in the resultant electrode (Fig. 1(c)).

3.2. Material characterization of I/NCB

To confirm the surface and bulk composition of I/NCB, the XPS and TGA were conducted and displayed in Fig. 2. Fig. 2(a) shows the core-level XPS spectra for C 1 s, N 1 s and F 1 s regions of CB, NCB, I/CB and I/NCB. It is clearly seen that the N 1 s and F 1 s peaks centered at 400 and 689 eV have developed for NCB and I/NCB, respectively. The carbon atoms adjacent to nitrogen dopants may serve as the strong adsorption sites with sulfonate anion groups in the PFSA ionomer [42]. Moreover,

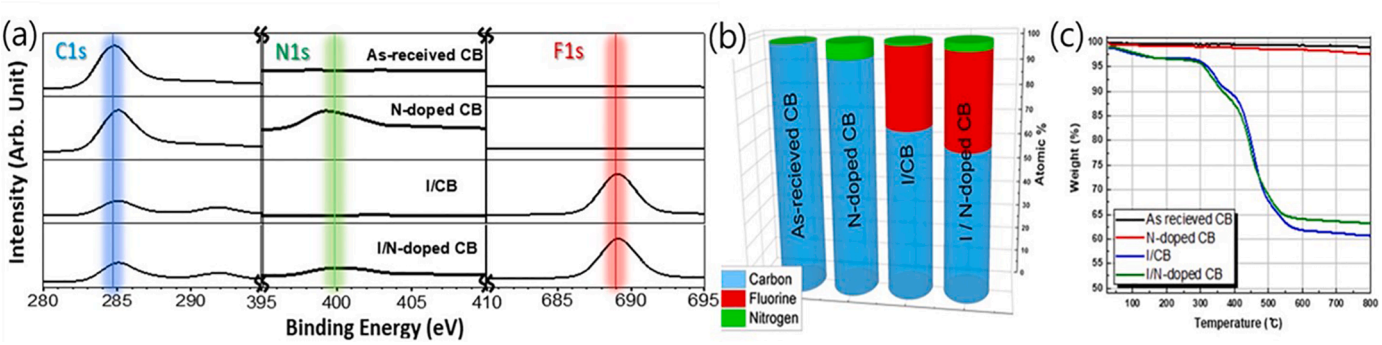

Fig. 2. XPS and TGA analyses on the as-received CB, NCB, I/CB and I/NCB – (a) C 1 s, N 1 s and F 1 s core-level XPS curves, (b) quantitative analysis on carbon, fluorine and nitrogen, and (c) TGA curve with N_2 feed gas.

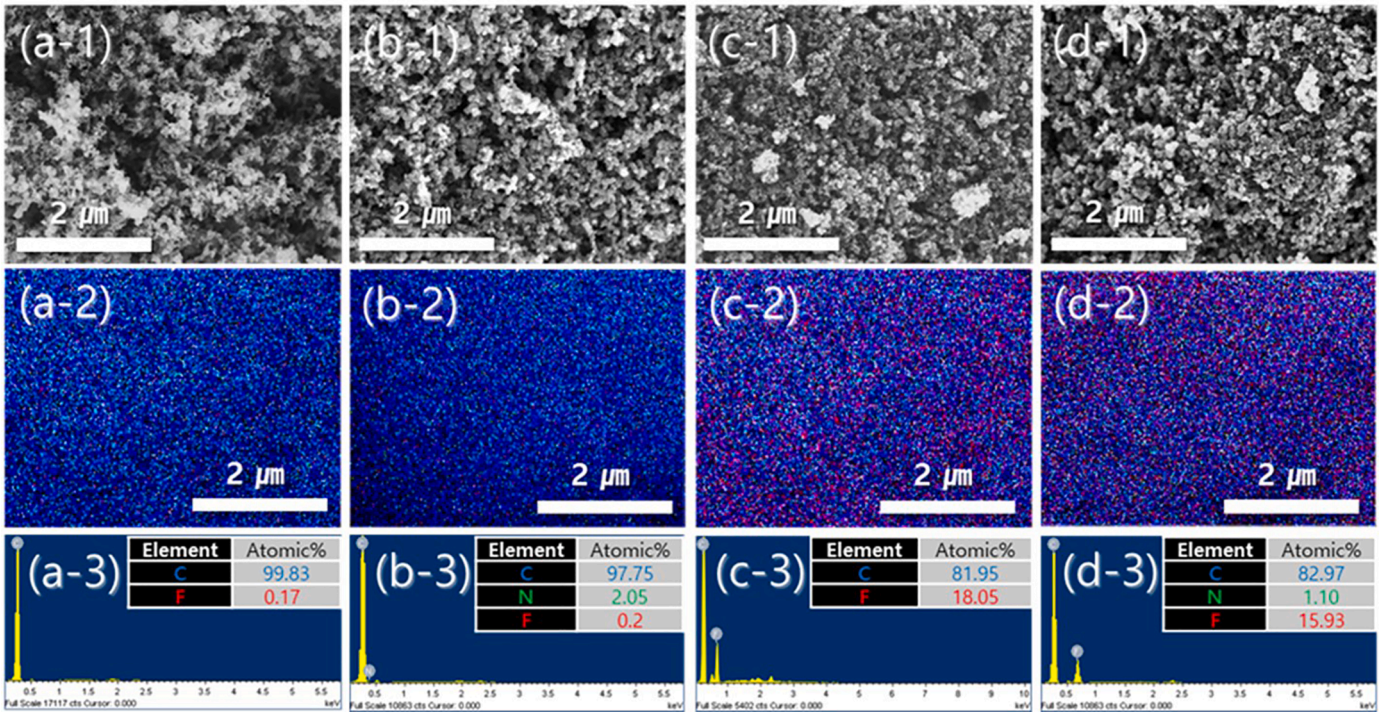

Fig. 3. SEM images on the top surfaces of cathode electrodes with elemental mapping and analyses on carbon (C), nitrogen (N) and fluorine (F) elements – (a) as-received CB, (b) NCB, (c) I/CB and (d) I/NCB.

the C1s peak centered at 285 eV, representing for sp2 carbon (including C=C, C-N, C-O and C=O), further diminished after the deposition of PFSA ionomer, indicating that the surface of NCB is massively covered by ionomer [27,43]. Fig. 2(b) provides the quantitative elemental analysis based on the atomic sensitive factors. In comparison between I/CB and I/NCB, the atomic composition of fluorine was recorded as considerably higher in I/NCB by approximately 6.2 at.%. However, the weight percentage of ionomer was remained similar to 35 wt.% as revealed from TGA data (Fig. 2(c)). Hence, it may be deduced that the PFSA ionomer is more uniformly distributed onto NCB than CB, that is attributed by the strong binding of ionomer onto the carbons nearby nitrogen atoms.

Fig. 3 shows the SEM images of as-received CB, NCB, I/CB and I/NCB with EDX mapping and analysis results, which reveals the amount and distribution of carbon, nitrogen and fluorine elements. As compared with CB, the nitrogen dopants are evenly located onto the surfaces of NCB at nitrogen content of 2.05 at.% (Fig. 3(a) and (b)). Only negligible amount of fluorine was detected in here. Subsequently, further evaluation was carried out after the ionomer is immobilized onto the CB and NCB, and presented in Fig. 3(c) and (d), respectively. Adequate amounts of fluorine were found for I/CB (18.05 at.%) and I/NCB (15.93 at.%), as the weight percentage of ionomer was fairly large up to 35 wt.% (Fig. 2 (c)). From comparison between the I/CB and I/NCB, it may be observed that the ionomer is rather homogeneously distributed onto NCB than CB. Typically, the white lumps in the SEM image, with magnifications ranging from x5,000 to x20,000, repeatedly reported as the ionomer aggregates [28,44,45]. However, it is impossible to provide an accurate comparison of the degree of ionomer distribution for the two samples; the primary particles of ionomer aggregate are extremely smaller than the field of view in the SEM analysis.

Thus, the morphology of I/NCB is further evaluated by TEM analysis combined with EDX surface mapping of carbon, nitrogen and fluorine elements, in order to identify the distribution of PFSA ionomer in the I/NCB in comparison with I/CB, as shown in Figs. 4 and 5. Multiple sites were explored to avoid the localization issue in the TEM analysis. Fig. 4a and b display that the diameters of as-received CB and NCB were ca. 30 to 40 nm, which correspond well with the typical morphology of Vulcan XC-72R [46]. After the deposition of ionomer, the diameters of I/CB and

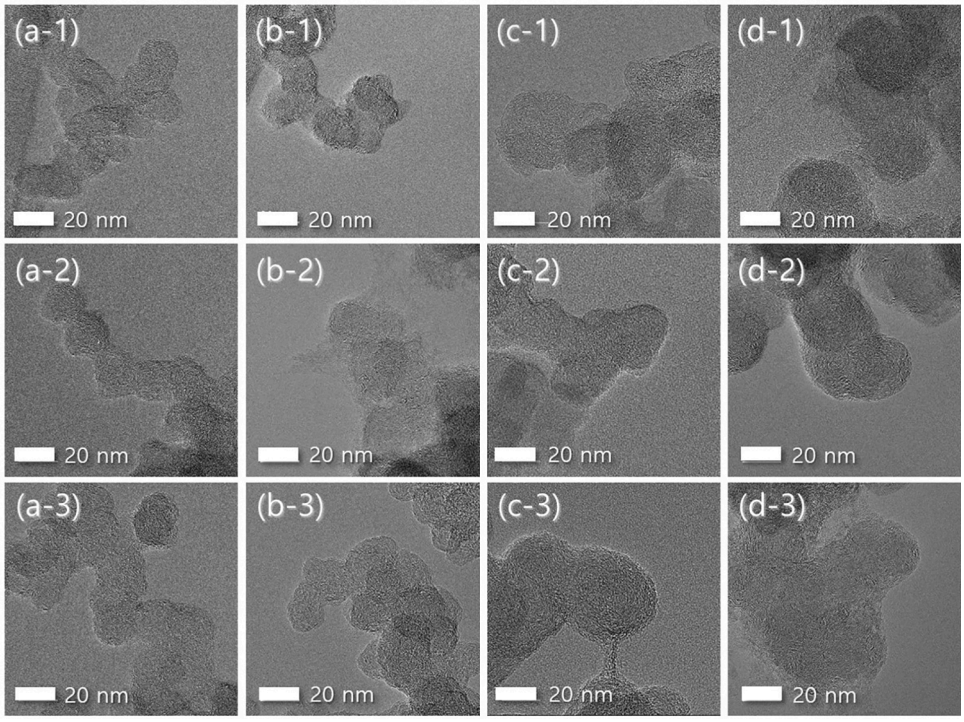

Fig. 4. TEM images on three different sites for evaluation of particle size distribution – (a) as-received CB, (b) NCB, (c) I/CB and (d) I/NCB.

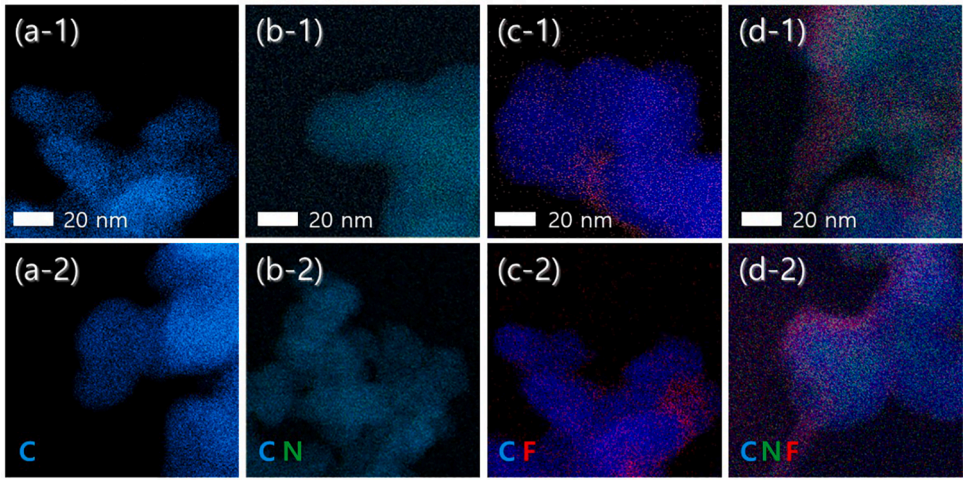

Fig. 5. STEM elemental mapping results on carbon (C), nitrogen (N) and fluorine (F) elements – (a) as-received CB, (b) NCB, (c) I/CB and (d) I/NCB on two different sites. The F is more homogeneously distributed onto the surface of I/NCB than I/CB.

I/NCB increased up to ca. 50 to 70 nm, indicating that ionomer layer with thickness ranging from 10 to 30 nm may be formed (Fig. 4c and d). The strand-shaped particles that interconnect the spherical-shaped particles are found in the both I/CB and I/NCB (Fig. 4(c-3) and (d-1)), which suggests the existence of sufficient ionomer [47]. The I/NCB showed more spherical-shaped particles with narrower particle size distribution when compared with I/CB. This may be attributed to a notably uniform distribution of ionomer, which can be further verified by the EDX mapping results. From the comparison between CB and NCB, the nitrogen atoms are uniformly distributed in the NCB throughout the carbon network, where the adjacent carbon atoms may act as strong binding sites for the ionomer (Fig. 5a and b) [48,49]. As observed from the surface mapping images of fluorine atoms, the I/NCB displayed a stronger locational correspondence among carbon, nitrogen and fluorine when compared with I/CB, where the ionomer layer is more uniformly distributed onto the surfaces of NCB (Fig. 5c and d). It is clearly shown that the I/CB exhibits a poor distribution of fluorine element with one or two largely agglomerated spots. Considering the severe aggregation of CB particles, the ionomer is more likely rather supported onto CB with different coverage ratios (simple-hybridized structure), than fully covered onto the external surfaces (core-shell-like structure). After the use of NCB, however, the sufficient numbers of carbon atoms adjacent to nitrogen dopant may attract the sulfonate groups in the sidechain of ionomer, due to the Coulombic interaction between them [27]. As a result, the ionomer coverage ratio is further increased with more uniform distribution, and the core-shell-like feature (fluorine elements are largely distributed on the shell region) is somewhat developed on several sites within I/NCB. Therefore, the TEM results are in good agreement with the XPS and TGA analyses, identifying that a uniform distribution of ionomer in I/NCB may be originated from

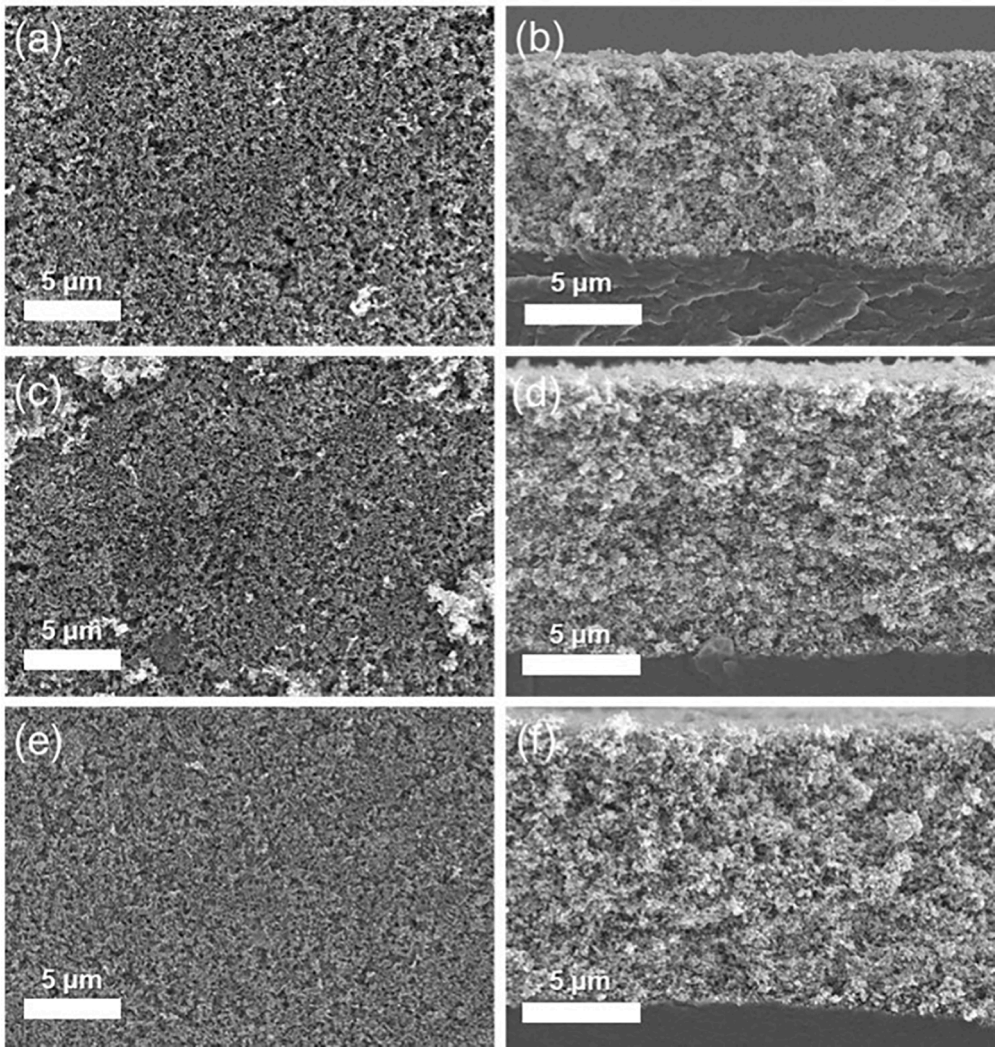

Fig. 6. SEM images on the top and cross-sectional surfaces of the cathode electrodes – SEM images of the conventional electrode (a and b) in comparison with the electrodes employing I/CB (c and d) and I/NCB (e and f).

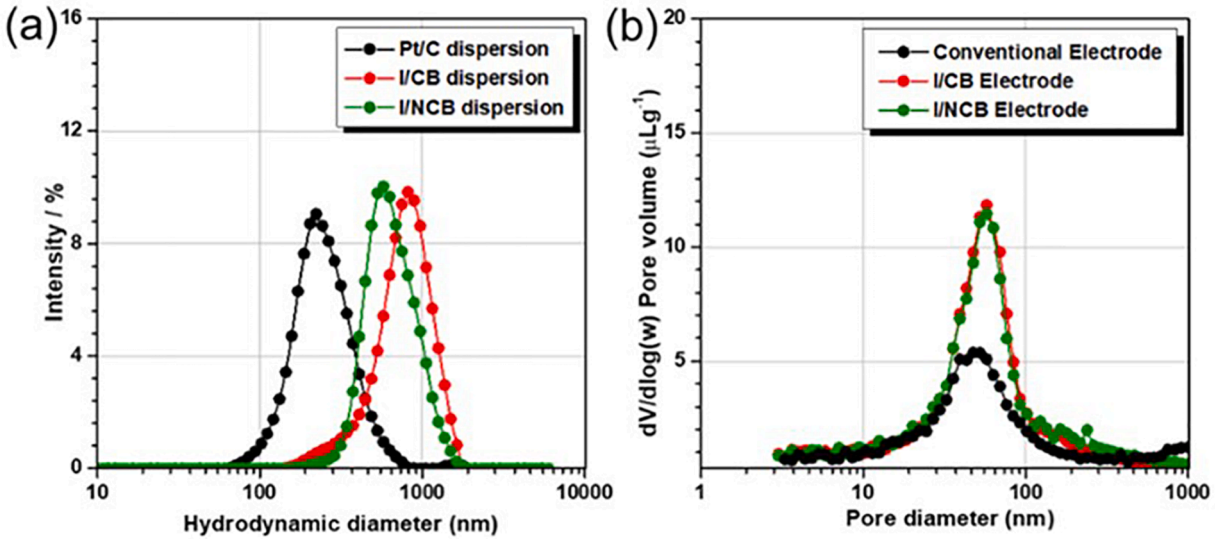

Fig. 7. Size distribution of the aggregates and electrode pores – (a) DLS data for the Pt/CB, I/CB and I/NCB, and (b) MIP data for the conventional electrode in comparison with the electrodes employing I/CB and I/NCB.

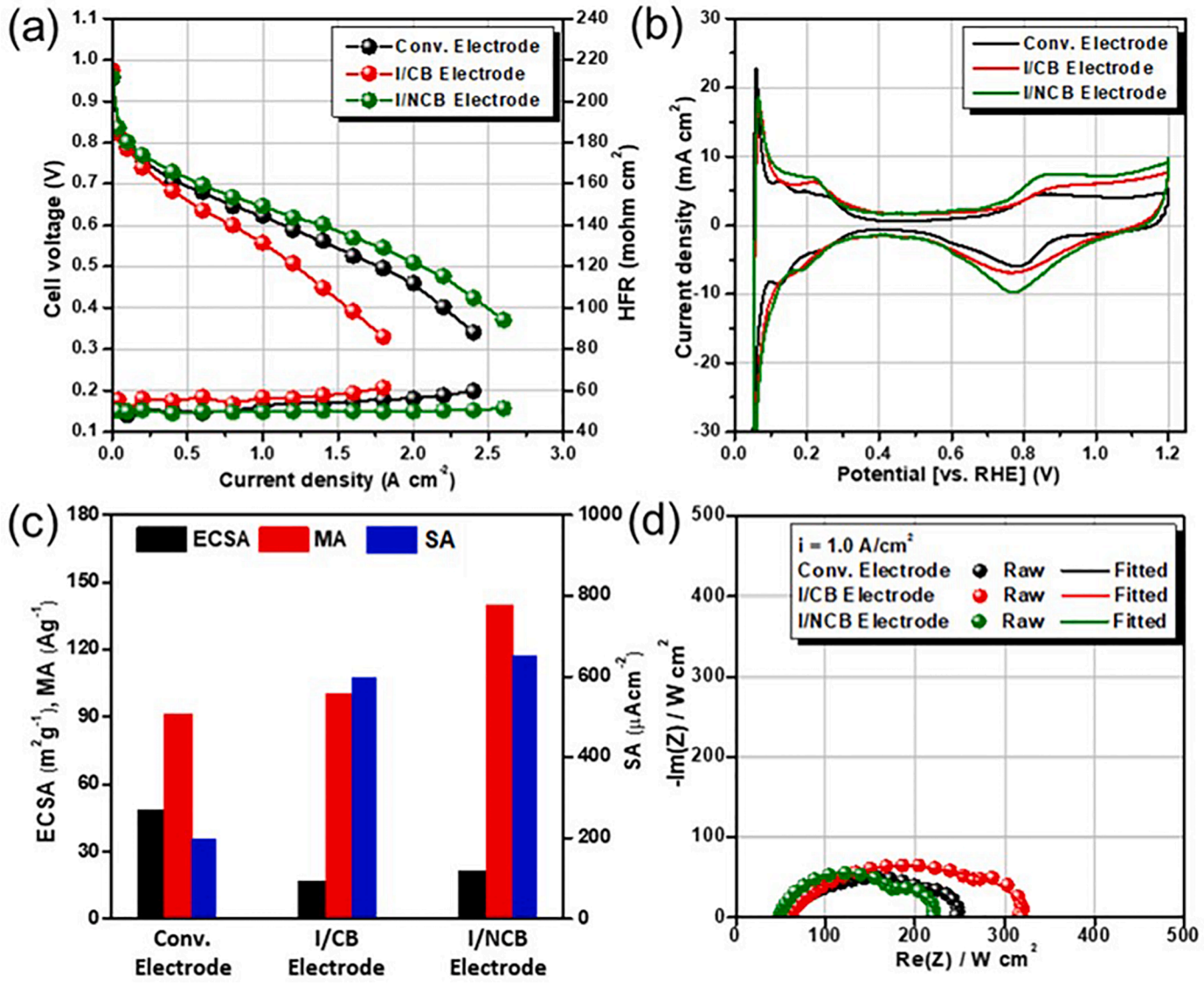

Fig. 8. Electrochemical properties of the PEFC electrodes employing I/CB and I/NCB when compared with the conventional one – (a) Cell polarization curve with high-frequency resistance, (b) CV, (c) quantitative analysis on ECSA, Pt mass activity (MA) and area-specific activity (SA), and (d) EIS nyquist plot at $i = 1.0$ A cm^{-2}.

the nitrogen dopants in NCB.

3.3. Characterization of the PEFC electrode employing I/NCB

Microstructures of the PEFC electrodes with the I/CB and I/NCB additives were compared with that of the conventional one, in order to investigate the effect of I/NCB as electrolyte and electrode binder. SEM images on top surface and cross section of the three electrodes are shown in Fig. 6. The conventional electrode exhibited a number of ionomer aggregates are quite evenly distributed in diameters ranging from 0.1 to 1 μm, where the average thickness of the electrode was 7.2 μm (Fig. 6(a) and (b)). The pores with diameters of several hundreds of nanometers can be observed. The diameters of ionomer aggregates became as large as 5 μm after the use of I/CB in the electrode; this indicates that a considerable amount of ionomer is detached from I/CB particle and takes part in enlarging the ionomer aggregates (Fig. 6(c)). In contrast, the electrode employing the I/NCB exhibited the most uniform distribution of ionomer among the three electrodes, with the average diameter of ionomer aggregates smaller than several tens of nanometer. Densely-packed electrode structure is successfully created with 40 nm large Pt/CB particles aggregated and surrounded by 50 to 60 nm large I/NCB. However, as shown in Fig. 6(d) and (f), the average thickness of electrode became larger up to 12.4 μm with porosity, that is primarily attributed by the additional amount of CB and NCB used in the I/CB and I/NCB, respectively.

For the further investigation on electrode pore structure, the MIP analysis was carried out in accordance with dynamic light scattering (DLS) measurement. As observed in Fig. 7(a), the size of primary aggregated particles is explored among Pt/CB, I/CB and I/NCB dispersed into the deionized water-IPA mixture solvent with identical composition used in the electrode slurry. The hydraulic diameters obtained from I/CB and I/NCB dispersions were significantly larger than that of the Pt/CB, with the peak intensities formed at 818 and 578 nm, respectively. Hence, a sufficient number of electrode pores with diameters ranging up to several tens of nanometers can be further created. This is well corresponded to the MIP data shown in Fig. 7(b). The electrode porosities are increased from 33.8% in the conventional electrode to 44.9% and 47.1% in the electrodes employing I/CB and I/NCB, where the increase of mercury intrusion volume is mainly associated by the pores with diameters ranging from 40 to 300 nm. This may compensate the negative effect of reduction in the electrode thickness on the O_2 transportation. In addition, the number counts of pores in smaller

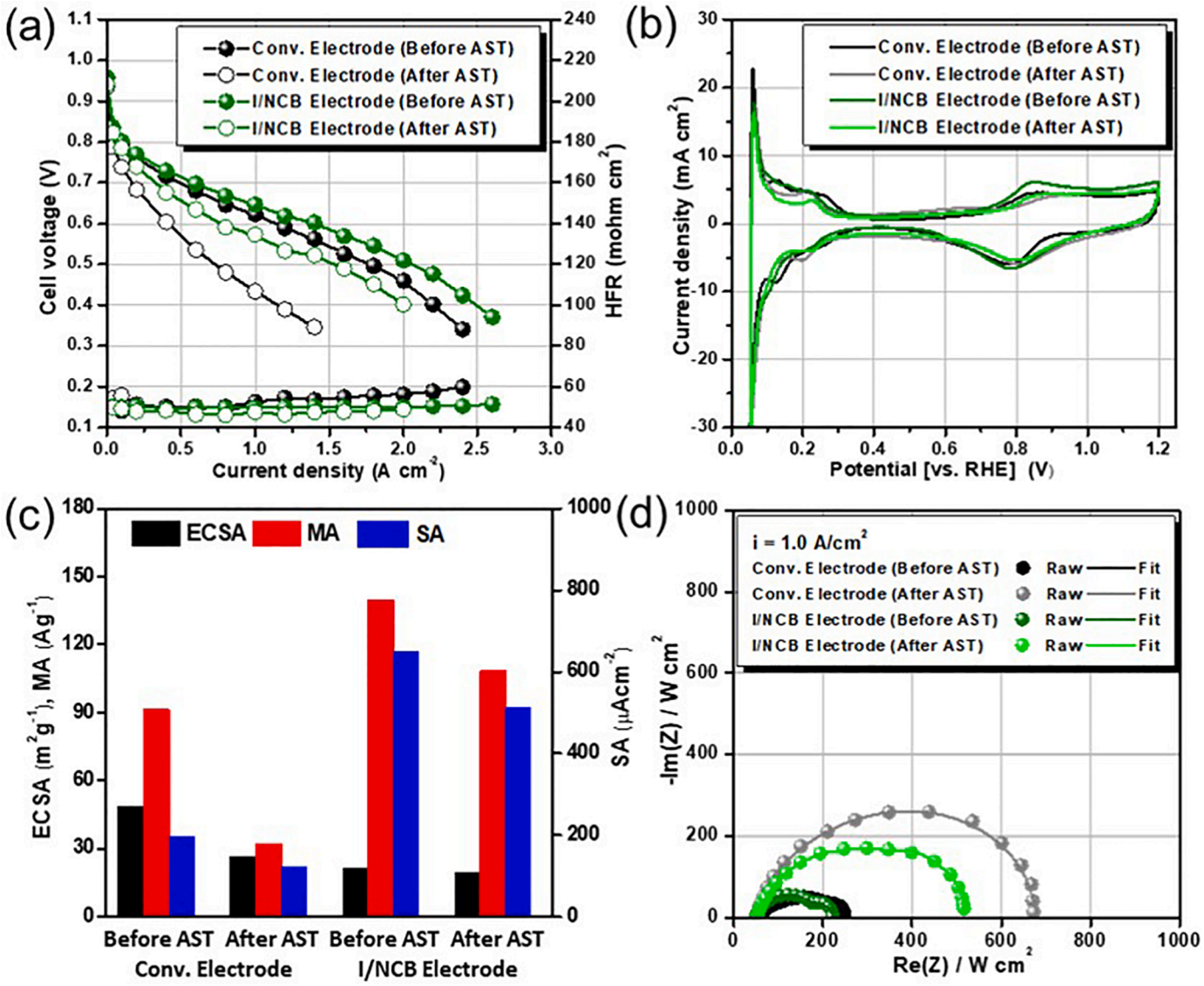

Fig. 9. Electrochemical properties of the PEFC with the conventional electrode and electrode employing I/NCBs after AST – (a) Cell polarization curve with high-frequency resistance, (b) CV, (c) quantitative analysis on ECSA, Pt mass activity (MA) and area-specific activity (SA), and (d) EIS nyquist plot at i = 1.0 A cm^{-2}.

diameters below 20 nm have slightly increased, due to the removal of ionomer in the inner region of Pt/CB aggregates [50,51]. Therefore, the resultant microstructure of electrode with I/NCB may be substantially advantageous in the O_2 mass transportation through the bulk pores as well as local ionomer layer enveloping Pt/CB.

3.4. *Fuel cell performance and durability*

The electrochemical performances of PEFC electrodes with I/CB and I/NCB are measured in comparison with the conventional one, by the direct-current polarization, CV, Pt mass and area-specific activity towards ORR, and EIS nyquist plot. As shown in Fig. 8(a), the PEFC electrode employing I/NCB presented the highest cell performance with a current density of 1.41 A cm^{-2} at 0.6 V, which resulted in 22.6% and 76.3% greater power density as compared with those having the conventional electrode and one employing I/CB, respectively. The high-frequency resistance (HFR) of electrode with I/CB was ca. 6 to 8 mΩ cm^2 larger, which corresponded with poor structural network of ionomer observed in the SEM image (Fig. 6(c)). From the CV curves, the peaks associated with electrical double layer charging and discharging, generated at the electrode potentials ranging from 0.4 to 0.6 V, are apparently increased after the use of electrodes employing I/CB and I/NCB (Fig. 8(b)). This is mainly attributed to the increase of interfacial area between ionomer and CB [52]. As the size of I/CB and I/NCB aggregates are significantly larger than Pt/CB, the ECSAs of electrodes with I/CB and I/NCB are found to be 65.4% and 55.8% smaller than that of the conventional electrode. The mass activity as well as area-specific activity towards ORR was extracted from Tafel data obtained under H_2-O_2 feed gas at an O_2 partial pressure of 1 atm [53], as presented in Fig. 8(c). The area-specific activity of electrode with I/NCB has reached triple times as high as that of the conventional one, thus exceeding the negative impact of ECSA degradation. To this end, the electrode kinetics towards ORR have dramatically improved with the mass activity of ca. 57% larger. Furthermore, the EIS analysis was conducted to show the O_2 mass-transport characteristics in the electrodes employing I/CB and I/NCB in comparison with the conventional electrode (Fig. 8(d)). While the HFR maintained at 49.8 to 56.4 mΩ cm^2, the electrode with I/NCB exhibited the lowest mass-transport resistance of 45.5 mΩ cm^2 that is dramatically reduced from those of the conventional electrode (65.9 mΩ cm^2) and one employing I/CBs (144.4 mΩ cm^2). This well corresponds to the degrees of ionomer distribution on the electrodes with I/CB and I/NCB, as discussed in the microstructural analyses (Fig. 6(c) and (e)).

Table 1
Summary on the electrochemical properties of resultant electrodes – ECSA, i-V performance and ORR mass activity at beginning-of-life and end-of-life stages.

Sample #	Configuration Catalyst	Ionomer	Beginning-of-life ECSA($m^2 g_{Pt}^{-1}$)	$i_{0.6V}^{perfor}$(Acm^{-2})	$i_{0.9V}^{mass}$(A g_{Pt}^{-1})	End-of-life ECSA($m^2 g_{Pt}^{-1}$)	$i_{0.6V}^{perfor}$(Acm^{-2})	$i_{0.9V}^{mass}$(A g_{Pt}^{-1})
Conv. Electrode	Pt/CB	PFSA Dispersion	48.6	1.15	91.3	26.6	0.42	32.4
I/CB Electrode	Pt/CB	I/CB	16.8	0.80	100.5	N/A	N/A	N/A
I/NCB Electrode	Pt/CB	I/NCB	21.5	1.41	139.6	19.2	0.79	108.4

Finally, we have evaluated the durability of PEFC electrode employing I/NCB by the AST for carbon support degradation, and presented in Fig. 9. The electrochemical properties of electrode having I/NCB before and after AST were compared with those of the conventional one, and summarized in Table 1. As shown in Fig. 9(a), the conventional electrode aggravated the cell current density from 1.15 down to 0.42 A cm^{-2} at 0.6 V, recording 63.5% of the performance decay. In contrast, the electrode with I/NCB exhibited less than 43% of the performance decay with the resultant current density of 0.79 A cm^{-2}. Notably enhanced durability of the electrode employing I/NCB may be primarily attributed to the anti-corrosive property of NCB. The CV curves have shown that the region representing for double layer charging/discharging has maintained similar peaks in the electrode employing the proposed electrode while displayed a notable reduction of the peak intensities in the conventional electrode; this suggests that less amount of degradation has occurred for the NCB supporting ionomer (Fig. 9(b)). As summarized in Fig. 9(c), the decay rate of ECSA was significantly smaller in the electrode employing I/NCB (10.8%) than conventional one (45.3%), although that of area-specific activity remained similar to 21 to 24.8%. This is mainly attributed by the significantly reduced amount of ionomer that is physically detached from NCB than carbon support in Pt/C catalyst after AST [54]. To this end, the mass activity of electrode with I/NCB resulted in a considerably higher value of 108.4 A g^{-1} even after AST, when compared with that of the conventional one (32.4 A g^{-1}). The EIS data are also displayed in Fig. 9(d), demonstrating that the resultant mass-transport resistance is apparently lower by 156 mΩ cm^2 in the electrode employing I/NCB when compared with the conventional electrode.

4. Conclusion

In this work, we have demonstrated a newly-structured PEFC electrode with I/NCB as electrolyte material for the enhanced cell performance and durability. To anchor and immobilize the PFSA ionomer onto carbon supports, NCB is prepared via a soft nitriding method that undergoes with aqueous solution of urea at lower reaction temperature at 400 °C. Unlike the previous electrode structure, the ionomer succeeded in developing a strong binding onto carbon atoms adjacent to nitrogen on the surfaces of NCB. As a result, a homogeneous distribution of ionomer is attained by controlling the agglomeration during the electrode coating and annealing processes; it is found to be significantly helpful in achieving higher ORR electrode kinetics and O_2 transport to the active sites. The dramatic improvements are achieved for the electrode mass activity on MEA scale and hence cell performance after the use of electrode employing I/NCB (139.6 A g^{-1} and 1.41 A cm^{-2}) when compared with the conventional electrode (91.3 A g^{-1} and 1.15 A cm^{-2}). Higher graphitization of NCB over CB also resulted in an excellent cell durability towards the carbon support degradation, with the 2.3-fold higher mass activity and 44.6% lower mass-transport resistance after AST. Based on these merits, the newly-proposed electrode architecture based on I/NCB may give an alternative pathway in obtaining the boosted ORR kinetics and O_2 transportation, along with an exceptional resistivity towards the carbon support degradation.

CRediT authorship contribution statement

Won Young Choi: Methodology, Investigation, Writing – original draft. **Dong Jun Seo:** Conceptualization, Investigation, Data curation. **Hyunguk Choi:** Investigation, Data curation. **Myeong Hwa Lee:** Methodology, Investigation. **Seo Won Choi:** Methodology, Investigation. **Young Gi Yoon:** Conceptualization, Writing – review & editing. **Tae Young Kim:** Visualization, Writing – review & editing. **Hansung Kim:** Conceptualization, Visualization, Writing – review & editing. **Chi-Young Jung:** Supervision, Funding acquisition, Writing – review & editing.

Declaration of Competing Interest

There are no conflicts to declare.

Acknowledgments

This research was supported by the Research and Development Innovation Valley Program through the Ministry of Science and ICT (2021-DD-RD-0202).

References

[1] T. Zhang, P. Wang, H. Chen, P. Pei, A review of automotive proton exchange membrane fuel cell degradation under start-stop operating condition, Appl. Energy 223 (2018) 249.
[2] I. Staffell, D. Scamman, A.V. Abad, P. Balcombe, P.E. Dodds, P. Ekins, N. Shah, W. R. Ward, The role of hydrogen and fuel cells in the global energy system, Energy Environ. Sci. 12 (2019) 463.
[3] D.A. Cullen, K.C. Neyerlin, R.K. Ahluwalia, R. Mukundan, K.L. More, R.L. Borup, A. Z. Weber, D.J. Myers, A. Kusoglu, New roads and challenges for fuel cells in heavy-duty transportation, Nat. Energy 6 (2021) 1.
[4] X.X. Wang, M.T. Swihart, G. Wu, Achievements, challenges and perspectives on cathode catalysts in proton exchange membrane fuel cells for transportation, Nat. Catal. 2 (2019) 578.
[5] A. Kusoglu, A.Z. Weber, New insights into perfluorinated sulfonic-acid ionomers, Chem. Rev. 117 (2017) 987.
[6] Y. Chang, Y. Qin, Y. Yin, J. Zhang, X. Li, Humidification strategy for polymer electrolyte membrane fuel cells – a review, Appl. Energy 230 (2018) 643.
[7] K. Kodama, K. Motobayashi, A. Shinohara, N. Hasegawa, K. Kudo, R. Jinnouchi, M. Osawa, Y. Morimoto, Effect of the side-chain structure of perfluoro-sulfonic acid ionomers on the oxygen reduction reaction on the surface of Pt, ACS Catal. 8 (2018) 694.
[8] Y.T. Mu, A.Z. Weber, Z.L. Gu, W.Q. Tao, Mesoscopic modeling of transport resistances in a polymer-electrolyte fuel-cell catalyst layer: analysis of hydrogen limiting currents, Appl. Energy 255 (2019), 113895.
[9] K. Karan, Interesting facets of surface, interfacial and bulk characteristics of perfluorinated ionomer films, Langmuir 35 (2019) 13489.
[10] J. Liu, T. Zhang, G.I.N. Waterhouse, Complex alloy nanostructures as advanced catalysts for oxygen electrocatalysis: from materials design to applications, J. Mater. Chem. A 8 (2020) 23142.
[11] J. Xie, F. Xu, D.L. Wood III, K.L. More, T.A. Zawodzinski, W.H. Smith, Influence of ionomer content on the structure and performance of PEFC membrane electrode assemblies, Electrochim. Acta 55 (2010) 7404.
[12] T. Kusano, T. Hiroi, K. Amemiya, M. Ando, T. Takahashi, M. Shibayama, Structural evolution of a catalyst ink for fuel cells during the drying process investigated by CV-SANS, Polym. J. 47 (2015) 546.
[13] C. Welch, A. Labouriau, R. Hjelm, B. Orler, C. Johnston, Y.S. Kim, Nafion in dilute solvent systems: dispersion or solution? ACS Macro Lett. 1 (2012) 1403.
[14] T.T. Ngo, T.L. Yu, H.L. Lin, Influence of the composition of isopropyl alcohol/water mixture solvents in catalyst ink solutions on proton exchange membrane fuel cell performance, J. Power Sources 225 (2013) 293.
[15] T.T. Ngo, T.L. Yu, H.L. Lin, Nafion-based membrane electrode assemblies prepared from catalyst inks containing alcohol/water solvent mixtures, J. Power Sources 238 (2013) 1.

[16] J. Xie, F. Garzon, T. Zawodzinski, W. Smith, Ionomer segregation in composite MEAs and its effect on polymer electrolyte fuel cell performance, J. Electrochem. Soc. 151 (2004) A1084.
[17] M.S. Saha, D.K. Paul, B.A. Peppley, K. Karan, Fabrication of catalyst-coated membrane by modified decal transfer technique, Electrochem. Commun. 12 (2010) 410.
[18] T.H. Kim, J.Y. Yi, C.Y. Jung, E. Jeong, S.C. Yi, Solvent effect on the Nafion agglomerate morphology in the catalyst layer of the proton exchange membrane fuel cells, Int. J. Hydrogen Energy 42 (2017) 478.
[19] R. Sharma, L. Grahl-Madsen, S.M. Andersen, Influence of dispersion media on Nafion ionomer distribution in proton exchange membrane fuel cell catalyst carbon support, Mater. Chem. Phys. 226 (2019) 66.
[20] A. Orfanidi, P.J. Rheinlander, N. Schulte, H.A. Gasteiger, Ink solvent dependence of the ionomer distribution in the catalyst layer of a PEMFC, J. Electrochem. Soc. 165 (2018) F1254.
[21] S. Shahgaldi, I. Alaefour, X. Li, The impact of short side chain ionomer on polymer electrolyte membrane fuel cell performance and durability, Appl. Energy 217 (2018) 295.
[22] T. Mashio, A. Ohma, T. Tokumasu, Molecular dynamics study of ionomer adsorption at a carbon surface in catalyst ink, Electrochim. Acta 202 (2016) 14.
[23] Y.C. Park, H. Tokiwa, K. Kakinuma, M. Watanabe, M. Uchida, Effects of carbon supports on Pt distribution, ionomer coverage and cathode performance for polymer electrolyte fuel cells, J. Power Sources 315 (2016) 179.
[24] V. Yarlagadda, M.K. Carpenter, T.E. Moylan, R.S. Kukreja, R. Koestner, W. Gu, L. Thompson, A. Kongkanand, Boosting fuel cell performance with accessible carbon mesopores, ACS Energy Lett. 3 (2018) 618.
[25] K. Miyazaki, N. Sugimura, K. Kawakita, T. Abe, K. Nishio, H. Nakanishi, M. Matsuoka, Z. Ogumi, Aminated perfluorosulfonic acid ionomers to improve the triple phase boundary region in anion-exchange membrane fuel cells, J. Electrochem. Soc. 157 (2010) A1153.
[26] A. Orfanidi, P. Madkikar, H.A. El-Sayed, G.S. Harzer, T. Kratky, H.A. Gasteiger, The key to high performance low Pt loaded electrodes, J. Electrochem. Soc. 164 (2017) F418.
[27] S. Ott, A. Orfanidi, H. Schmies, B. Anke, H.N. Nong, J. Hübner, U. Gernert, M. Gliech, M. Lerch, P. Strasser, Ionomer distribution control in porous carbon-supported catalyst layers for high-power and low Pt-loaded proton exchange membrane fuel cells, Nat. Mater. 19 (2020) 77.
[28] C.Y. Ahn, J. Ahn, S.Y. Kang, O.H. Kim, D.W. Lee, J.H. Lee, J.G. Shim, C.H. Lee, Y. H. Cho, Y.E. Sung, Enhancement of service life of polymer electrolyte fuel cells through application of nanodispersed ionomer, Sci. Adv. 6 (2020) eaaw0870.
[29] S.M. Anderson, R. Dhiman, M.J. Larsen, E. Skou, Importance of electrode hot-pressing conditions for the catalyst performance of proton exchange membrane fuel cells, Appl. Catal. B-Environ. 172 (2015) 82.
[30] S. Shahgaldi, I. Alaefour, X. Li, Impact of manufacturing processes on proton exchange membrane fuel cell performance, Appl. Energy 225 (2018) 1022.
[31] S. Takahashi, J. Shimanuki, T. Mashio, A. Ohma, H. Tohma, A. Ishihara, Y. Ito, Y. Nishino, A. Miyazawa, Observation of ionomer in catalyst ink of polymer electrolyte fuel cell using cryogenic transmission electron microscopy, Electrochim. Acta 224 (2017) 178.
[32] O.J. Curnick, B.G. Pollet, P.M. Mendes, Nafion®-stabilised Pt/C electrocatalysts with efficient catalyst layer ionomer distribution for proton exchange membrane fuel cells, RSC Adv. 2 (2012) 8368.
[33] B. Liu, H. Yao, W. Song, L. Jin, I.M. Mosa, J.F. Rusling, S.L. Suib, J. He, Ligand-free noble metal nanocluster catalysts on carbon supports via "soft" nitriding, J. Am. Chem. Soc. 138 (2016) 4718.
[34] J. Fan, M. Chen, Z. Zhao, Z. Zhang, S. Ye, S. Xu, H. Wang, H. Li, Bridging the gap between highly active oxygen reduction reaction catalysts and effective catalyst layers for proton exchange membrane fuel cells, Nat. Energy 6 (2021) 475.
[35] M.S. Wilson, S. Gottesfeld, High performance catalyzed membranes of ultra-low Pt loadings for polymer electrolyte fuel cells, J. Electrochem. Soc. 139 (1992) L28.
[36] J. Xie, K.L. More, T.A. Zawodzinski, W.H. Smith, Porosimetry of MEAs made by "thin film decal" method and its effect on performance of PEFCs, J. Electrochem. Soc. 151 (2004) A1841.
[37] H. Lee, S. Park, H. Kim, Preparation of CO-tolerant PtRuNi/C ternary electrocatalyst having a composition gradient shell, Chem. Eng. J. 414 (2021), 128792.
[38] H. Choi, D.J. Seo, W.Y. Choi, M.H. Lee, Y.J. Park, T.Y. Kim, Y.G. Yoon, S.C. Yi, C. Y. Jung, An ultralight-weight polymer electrolyte fuel cell based on woven carbon fiber-resin reinforced bipolar plate, J. Power Sources 484 (2021), 229291.
[39] Q. Zhang, M. Schulze, P. Gazdzicki, A. Friedrich, Comparison of different performance recovery procedures for polymer electrolyte membrane fuel cells, Appl. Energy 302 (2021), 117490.
[40] C.Y. Jung, S.W. Choi, W.Y. Choi, C.W. Hong, V.R. Jothi, S.C. Yi, Engineering ionomer homogeneously distributed onto the fuel cell electrode with superbly retrieved activity towards oxygen reduction reaction, Appl. Catal. B-Environ. 298 (2021), 120609.
[41] M. Lopez-Haro, L. Guétaz, T. Printemps, A. Morin, S. Escribano, P.H. Jouneau, P. Bayle-Guillemaud, F. Chandezon, G. Gebel, Three-dimensional analysis of Nafion layers in fuel cell electrodes, Nat. Commun. 5 (2014) 5229.
[42] D.W. Lee, J.H. Jang, I. Jang, Y.S. Kang, S. Jang, K.Y. Lee, J.H. Jang, H.J. Kim, S. J. Yoo, Bio-derived Co_2P nanoparticles supported on nitrogen-doped carbon as promising oxygen reduction reaction electrocatalyst for anion exchange membrane fuel cells, Small 15 (2019), 1902090.
[43] Q. Lv, W. Si, J. He, L. Sun, C. Zhang, N. Wang, Z. Yang, X. Li, X. Wang, W. Deng, Y. Long, C. Huang, Y. Li, Selectively nitrogen-doped carbon materials as superior metal-free catalysts for oxygen reduction, Nat. Commun. 9 (2018) 3376.
[44] K. Kakinuma, M. Kawamoto, K. Tamoto, M. Yamaguchi, S. Honmura, A. Iiyama, M. Uchida, Evaluation of ionomer distribution on electrocatalysts for polymer electrolyte fuel cells by use of a low acceleration voltage scanning electron microscope, J. Electrochem. Soc. 168 (2021), 054510.
[45] M. Harada, S. Takata, H. Iwase, S. Kajiya, H. Kadoura, T. Kanaya, Distinguishing adsorbed and deposited ionomers in the catalyst layer of polymer electrolyte fuel cells using contrast-variation small-angle neutron scattering, ACS Omega 6 (2021) 15257.
[46] N.E. Souza, J.L. Bott-Neto, T.A. Rocha, G.C. da Silva, E. Teixeira-Neto, E. R. Gonzalez, E.A. Ticianelli, Support modification in Pt/C electrocatalysts for durability increase: a degradation study assisted by identical location transmission electron microscopy, Electrochim. Acta 265 (2018) 523.
[47] D.A. Cullen, R. Koestner, R.S. Kukreja, Z.Y. Liu, S. Minko, O. Trotsenko, A. Tokarev, L. Guetaz, H.M. Meyer III, C.M. Parish, K.L. More, Imaging and microanalysis of thin ionomer layers by scanning transmission electron microscopy, J. Electrochem. Soc. 161 (2014) F1111.
[48] T. Kondo, S. Casolo, T. Suzuki, T. Shikano, M. Sakurai, Y. Harada, M. Saito, M. Oshima, M.I. Trioni, G.F. Tantardini, J. Nakamura, Atomic-scale characterization of nitrogen-doped graphite: effects of dopant nitrogen on the local electronic structure of the surrounding carbon atoms, Phys. Rev. B 86 (2012), 035436.
[49] D. Guo, R. Shibuya, C. Akiba, S. Saji, T. Kondo, J. Nakamura, Active sites of nitrogen-doped carbon materials for oxygen reduction reaction clarified using model catalysts, Science 351 (2016) 361.
[50] Y. Hou, H. Deng, F. Pan, W. Chen, Q. Du, K. Jiao, Pore-scale investigation of catalyst layer ingredient and structure effect in proton exchange membrane fuel cell, Appl. Energy 253 (2019), 113561.
[51] S. Shukla, F. Wei, M. Mandal, J. Zhou, M.S. Saha, J. Stumper, M. Secanell, Determination of PEFC gas diffusion layer and catalyst layer porosity utilizing archimedes principle, J. Electrochem. Soc. 166 (2019) F1142.
[52] Z. Fang, A.G. Star, T.F. Fuller, Effect of carbon corrosion on wettability of PEM fuel cell electrodes, J. Electrochem. Soc. 166 (2019) F709.
[53] D.W. Banham, J.N. Soderberg, V.I. Birss, Pt/carbon catalyst layer microstructural effects on measured and predicted Tafel slopes for the oxygen reduction reaction, J. Phys. Chem. C 113 (2009) 10103.
[54] L. Castanheira, W.O. Silva, F.H.B. Lima, A. Crisci, L. Dubau, F. Maillard, Carbon corrosion in proton-exchange membrane fuel cells: effect of the carbon structure, the degradation protocol, and the gas atmosphere, ACS Catal. 5 (2015) 2184.